

The discovery and characterization of (594913) 'Ayló'chaxnim, a kilometre sized asteroid inside the orbit of Venus

Bryce T. Bolin^{1,2★}, T. Ahumada³, P. van Dokkum⁴, C. Fremling¹, M. Granvik^{5,6}, K. K. Hardegree-Ullman^{7†}, Y. Harikane^{8,9}, J. N. Purdum¹⁰, E. Serabyn¹¹, J. Southworth¹² and C. Zhai¹¹

¹*Division of Physics, Mathematics and Astronomy, California Institute of Technology, Pasadena, CA 91125, USA*

²*Infrared Processing and Analysis Center, California Institute of Technology, Pasadena, CA 91125, USA*

³*Department of Astronomy, University of Maryland, College Park, MD 20740, USA*

⁴*Department of Astronomy, Yale University, New Haven, CT 06511, USA*

⁵*Department of Physics, University of Helsinki, FI-00560, Helsinki, Finland*

⁶*Asteroid Engineering Lab, Luleå University of Technology, SE-981 28 Kiruna, Sweden*

⁷*Steward Observatory, University of Arizona, Tucson, AZ 85721, USA*

⁸*Institute for Cosmic Ray Research, The University of Tokyo Kashiwa, Chiba 277-8582, Japan*

⁹*National Astronomical Observatory of Japan, Tokyo, 181-8588, Japan*

¹⁰*Caltech Optical Observatory, California Institute of Technology, Pasadena, CA 91125, USA*

¹¹*Jet Propulsion Laboratory, California Institute of Technology, Pasadena, CA 91109, USA*

¹²*Astrophysical Research Institute, Liverpool John Moores University, Liverpool L2 2QP, UK*

Accepted 2022 August 4. Received 2022 August 3; in original form 2022 July 14

ABSTRACT

Near-Earth asteroid population models predict the existence of bodies located inside the orbit of Venus. Despite searches up to the end of 2019, none had been found. We report discovery and follow-up observations of (594913) 'Ayló'chaxnim, an asteroid with an orbit entirely interior to Venus. (594913) 'Ayló'chaxnim has an aphelion distance of ~ 0.65 au, is ~ 2 km in diameter and is red in colour. The detection of such a large asteroid inside the orbit of Venus is surprising given their rarity according to near-Earth asteroid population models. As the first officially numbered and named asteroid located entirely within the orbit of Venus, we propose that the class of interior to Venus asteroids be referred to as 'Ayló'chaxnim asteroids.

Key words: minor planets, asteroids: general.

1 INTRODUCTION

Almost all of the ~ 1 million known asteroids are located on orbits exterior to Earth's orbit compared to just a fraction of a per cent that have orbits located entirely inside Earth's orbit (Binzel, Reddy & Dunn 2015). Dynamical models predict that a small fraction of the near-Earth asteroid (NEA) population (Bottke et al. 2002; Granvik et al. 2018) consists of Atira asteroids located between the orbit of the Earth and Venus, and inner-Venus asteroids (IVAs) located entirely within the orbit of Venus. However, IVAs have not been observed despite previous searches for objects interior to the orbit of the Earth (Whiteley & Tholen 1998; Zavadny et al. 2008; Bolin et al. 2022). This is in part due to the difficulty of surveying this region of the Solar system within a small angular distance of the Sun with ground-based telescopes (Masi 2003). This postulated IVA population has been provisionally referred to as Vativas,¹ by analogy with the Atiras (Greenstreet et al. 2012).

* E-mail: bolin.astro@gmail.com

† Visiting astronomer, Cerro Tololo Inter-American Observatory at NSF's NOIRLab, which is managed by the Association of Universities for Research in Astronomy (AURA) under a cooperative agreement with the National Science Foundation.

¹ 'Provisional because it will be abandoned once the first discovered member of this class will be named' (Greenstreet, Ngo & Gladman 2012).

The Zwicky Transient Facility (ZTF) mounted on the Palomar Observatory Samuel Oschin Schmidt Telescope is an all-sky survey designed to detect transients in the Northern hemisphere (Bellm et al. 2019a; Bolin et al. 2022). A portion of the time for the ZTF survey is designed to observe portions of the sky as close as possible to the Sun during evening and morning twilight called the 'Twilight Survey' (Bolin et al. 2022). A preliminary version of the Twilight Survey ran in late 2018 and the first half of 2019 (Ye et al. 2020). An expanded version of the Twilight Survey was executed between 2019 September 20 and 2020 January 30, observing during astronomical twilight on each clear night.

2 OBSERVATIONS

The Twilight Survey is scheduled within the framework of the ZTF scheduler (Bellm et al. 2019b). The Twilight Survey alternates between evening and morning twilight providing a total of 90 observing sessions, on 47 mornings and on 43 evenings between 2019 September 20 and 2020 January 30. The scheduler produces a nearly connecting 10 field pattern that covers 470 square degrees of sky during each observing session at elevations down to ~ 20 deg. Each Twilight Survey session lasts for 20–25 min. Each field in the pattern is imaged four times with 30 s exposures in *r*-band (wavelength ~ 680 nm) (Bellm et al. 2019b). The time between subsequent exposures per single Twilight Survey fields is ~ 5 min. The time

spacing of the Twilight Survey cadence enables the detection of objects moving in the range between ~ 8 arcsec per hour and > 1500 arcsec per hour (Dueb et al. 2019; Masci et al. 2019).

The sensitivity of the Twilight Survey images is brighter than the nominal ZTF limiting V-band (wavelength ~ 550 nm) magnitude of ~ 21 (Bellm et al. 2019a). The brighter sensitivity is due to the higher airmass of the observations combined with the higher sky background during astronomical twilight, resulting in a limiting magnitude close to $V \sim 20$ (fig. A1, Bolin et al. 2022). A total of $\sim 40\,000$ sq. deg. sky was covered during the Twilight Survey between 2019 September to 2020 January. A sky coverage map of the 90 Twilight Survey observing sessions is presented in Fig. 1(A). The apparent asymmetry between the morning and evening patches is due to differences in the accessibility of the sky in the Sun's direction during evening and morning twilight during the September to January months. The solar elongation of the sky covered by the Twilight Survey ranged between 35 and 60 deg (Fig. 1B). Approximately half of the sky covered by the Twilight Survey is within the IVA maximum solar elongation range of < 46 deg (Fig. 1B). The NEA model (Granvik et al. 2018) predicts that ~ 80 per cent of IVAs have a maximum Solar elongation overlapping with the solar elongation range covered by the Twilight Survey (Fig. 1C).

3 RESULTS

3.1 Initial detection

On 2020 January 4, 2020 AV₂ was detected by ZTF in the evening twilight sky ~ 40 deg from the Sun (Fig. 1A,B, Fig. 2A,B). Follow-up data were obtained with the Kitt Peak Electron Multiplying Charge-Coupled Device Demonstrator (KPED) mounted on the Kitt Peak 84-inch telescope (Coughlin et al. 2019) on 2020 January 9 and were reported to the Minor Planet Center (MPC). The astrometry from the follow-up observations combined with the initial ZTF observations refined the aphelion, Q , of 2020 AV₂ as having a value of ~ 0.65 astronomical units (au), well within the 0.72 au perihelion, q , of Venus, as seen in the top and bottom panels of Fig. 3 (Bolin et al. 2020).

Follow-up data from other observatories were reported during 2020 January 4–23 resulting in a more precise orbit fit with $Q = 0.653817 \pm 0.000825$ au. The orbit of 2020 AV₂ was further refined when recovery observations were taken by follow-up observers during its next window of observability from the Northern hemisphere in 2020 November 24–26 and reported to the MPC.² These additional recovery observations extended the observing span to 327 d improving the precision of 2020 AV₂'s orbital elements to one part in a million (table A1, Bolin et al. 2022). A third set of observations confirming the orbit were obtained in 2021 July 17–19 at the Southern Astrophysical Research Telescope and Magellan Telescope (Fig. 2C; Bolin et al. 2022). The more precise orbit fit enabled by these three epochs of observations resulted in 2020 AV₂ receiving the number designation (594913) 'Ayló'chaxnim by the MPC on 2021 September 20 (Payne et al. 2021). On 2021 November 8, the International Astronomical Union Working Group on Small Body Nomenclature officially named the asteroid 'Ayló'chaxnim, meaning 'Venus Girl' in the Luiseño language (Tichá et al. 2021). We suggest that the class of interior to Venus asteroids be referred to as 'Ayló'chaxnim following the example of (594913) 'Ayló'chaxnim as the first known example of this class of asteroids.

²https://minorplanetcenter.net/db_search/show_object?object_id=K20A02V

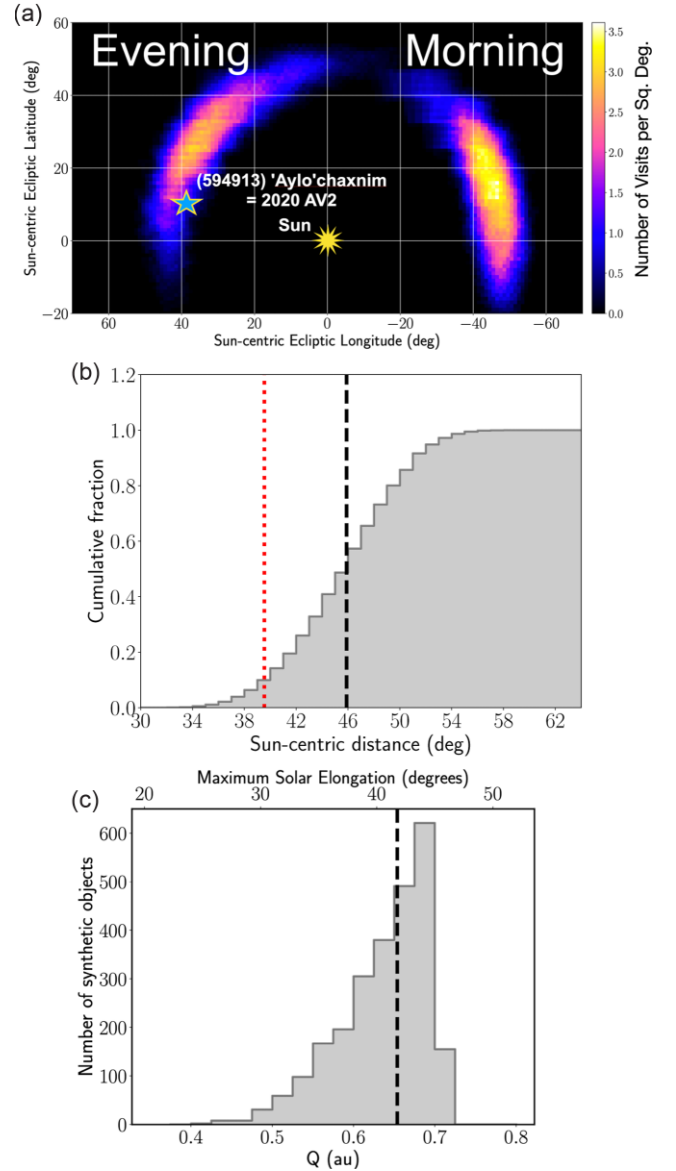


Figure 1. ZTF Twilight Survey sky coverage. (A) Sun-centric sky distribution of Twilight Survey coverage between 2019 September 19 and 2020 January 30. The blue star indicates the first observed location of 'Ayló'chaxnim and the yellow star indicates the Sun. The colour scale is the number of ZTF visits per square degree. (B) Cumulative distribution of the Sun-centric distance of the Twilight survey footprints in the same time period. The vertical black dashed line shows the maximum possible Sun-centric distance of inner-Venus objects and the vertical red dotted line shows the Sun-centric distance of 'Ayló'chaxnim when it was first observed on 2022 January 4. (C) Maximum solar distance, Q , distribution using synthetic inner-Venus objects generated from the NEA model. The vertical dashed line shows the aphelion of 'Ayló'chaxnim. The upper x-axis shows the maximum solar elongation of the synthetic inner-Venus object population.

3.2 Orbital dynamics

Previous simulations of the orbital evolution of 'Ayló'chaxnim (de la Fuente Marcos & de la Fuente Marcos 2020; Greenstreet 2020) indicate its capture into orbital period resonances with Venus, such as the 3:2 mean motion resonance located at 0.552 au. We performed further orbital stability simulations using the orbital solution of 'Ayló'chaxnim from 2020 November, finding that the nominal

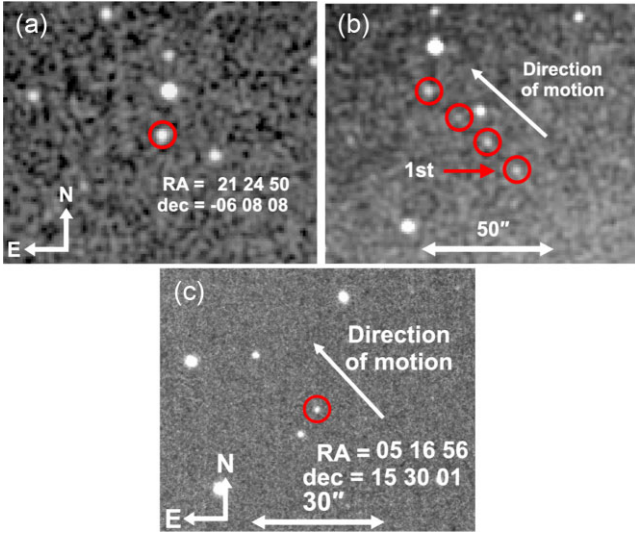


Figure 2. ZTF images of 'Ayló'chaxnim. (A) One of the ZTF discovery 30 s *r*-band images of 'Ayló'chaxnim taken on 2020 January 4. 'Ayló'chaxnim is indicated by the red circle. (B) Composite image of the first four ZTF 30 s *r*-band exposures over a 22 min time interval. The images were aligned on the background stars before being coadded. 'Ayló'chaxnim is indicated by the red circles, with the first observation labelled with a red arrow. The apparent faintness of the third detection is due to variations in sky transparency over the 22 min sequence. The asteroid was moving ~ 130 arcsec per hour in the northeast direction resulting in a ~ 10 arcsec spacing between the detections of 'Ayló'chaxnim. The spatial scale in (B) is the same as in (A). (C) Recovery image of 'Ayló'chaxnim made using the 6.5 m Magellan Baade telescope and Four Star infrared camera on 2021 July 18. The asteroid was moving in the northeast direction at 100 arcsec per hour. The cardinal directions are indicated.

orbit of 'Ayló'chaxnim enters the 3:2 mean motion with Venus ~ 0.06 Myr from now (Fig. 4A). The amplitude of the variations in the semimajor axis, a , of 'Ayló'chaxnim is initially large but shrinks after close encounters with Mercury ~ 0.01 Myr later. The minimum approach distance between 'Ayló'chaxnim and Venus increases when 'Ayló'chaxnim enters into this resonance, thereby protecting the asteroid from close encounters with the planet (similar to the 3:2 mean motion resonances between Neptune and Pluto; Nesvorný, Roig & Ferraz-Mello 2000). The integration of the majority of our orbital clones indicates that the asteroid 'Ayló'chaxnim will remain in resonance with Venus for ~ 0.01 Myr, and subsequently leave and re-enter the 3:2 mean motion resonance for the next ~ 0.1 Myr.

Our orbital evolution simulations also indicate that 'Ayló'chaxnim has only recently migrated entirely inside the orbit Venus, within the last ~ 1 Myr, remaining inside the orbit of Venus for another ~ 2 Myr (Fig. 4B). The proximity of the perihelion of 'Ayló'chaxnim to the orbit of Mercury draws comparison with the perihelia of many ecliptic comets being close to the orbit of Jupiter, indicative of the evolution of their orbits due to close planetary encounters (Duncan, Levison & Dones 2004). The orbit of 'Ayló'chaxnim will have aphelia within the orbit of Venus for the next 2 Myr. Previous simulations found a much shorter residence time of < 1 Myr for 'Ayló'chaxnim to remain inside the orbit of Venus (de la Fuente Marcos & de la Fuente Marcos 2020; Greenstreet 2020). We ascribe the differences with our results as due to previous work adopting an earlier version of the orbital parameters for 'Ayló'chaxnim.

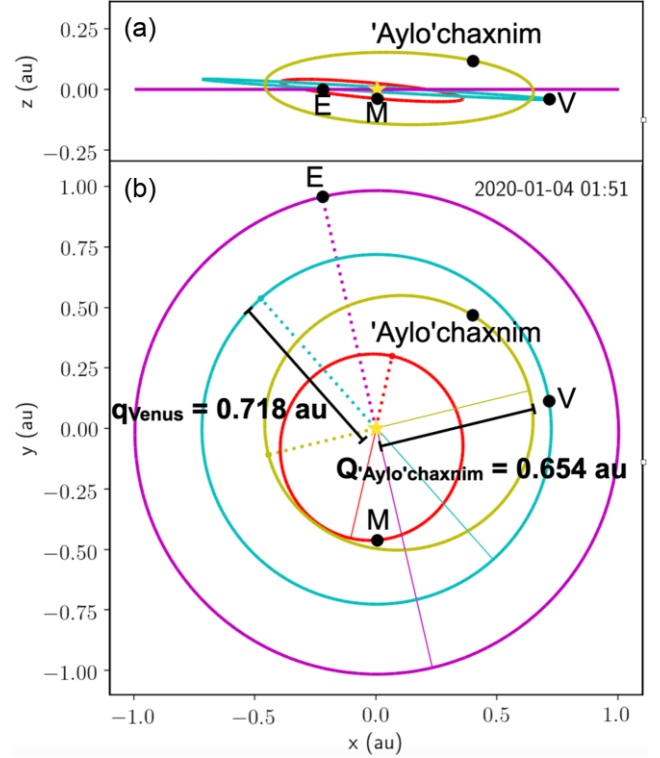


Figure 3. Orbital configuration of 'Ayló'chaxnim. (A) A side view of the plane of the Solar system. The orbits and locations of Earth (purple), Venus (blue), Mercury (red), and 'Ayló'chaxnim (yellow) on 2020 January 4 are shown looking from the side. (B) The same as panel (A) but looking from above the orbital plane of the inner Solar system. The perihelion and aphelion directions of 'Ayló'chaxnim and the planets are plotted with dotted and solid lines, respectively. The perihelion distance of Venus, $q_{\text{Venus}} = 0.718$ au, and the aphelion distance of 'Ayló'chaxnim, $Q_{\text{'Ayló'chaxnim}} = 0.654$ au, are indicated with labelled barred lines. The heliocentric Cartesian coordinates x , y , and z are indicated with the position of the Sun as the origin.

While the current precision of 'Ayló'chaxnim's orbit prevents us from predicting its orbital behaviour on time-scales exceeding ~ 10 Myr, it is apparent from orbital integration of clones (see section A1.3, Bolin et al. 2022) of its orbit that it is a transitory inhabitant of the inner Venus region of the Solar system. The majority of orbital clones have close encounters with Mercury, Venus and the Earth within 10–20 Myr that scatter and evolve their orbits on to excited trajectories that have very close perihelion passages with the Sun (Fig. 4C). The median time between the start time of the integration of the 'Ayló'chaxnim clones and their collision with a planet or the Sun is ~ 10 Myr, and ~ 90 per cent of the clones have collided with the Sun or a planet by the end of the 30 Myr integration. We integrated the ~ 10 per cent of clones that survived the first 30 Myr for a total of 50 Myr. On that time-scale, ~ 13 per cent of the 'Ayló'chaxnim clones collided with the Sun, having a perihelion distance < 0.005 au, while 13 per cent, 52 per cent, 16 per cent, and 2 per cent collided with Mercury, Venus, the Earth, and Mars, respectively. The remaining 4 per cent survived the extended 50 Myr integration or were ejected from the Solar system. Previous simulations of inner-Venus objects found a median collisional lifetime of ~ 21 Myr (Greenstreet et al. 2012), a factor of 2 larger than we find for 'Ayló'chaxnim clones. However, the proportion of 'Ayló'chaxnim clones colliding with the Sun, Mercury,

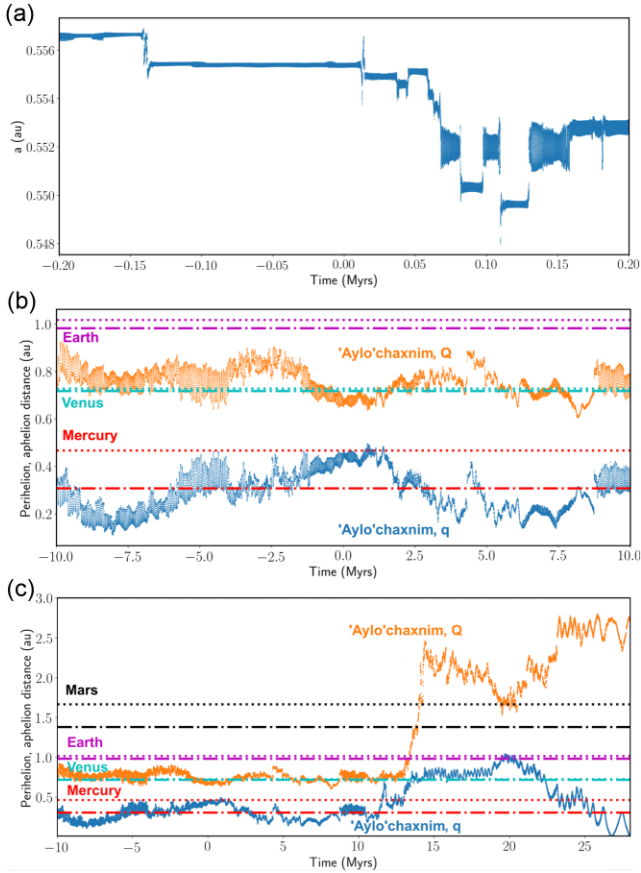


Figure 4. Orbital evolution of a synthetic clone representing the nominal orbit of 'Ayló'chaxnim. (A) Evolution of the semimajor axis of 'Ayló'chaxnim represented by its nominal orbit in table A1. The plateaus in the evolution of the semimajor axis separated by jumps are due to 'Ayló'chaxnim crossing different resonances with Venus. At around 0.06 Myr, 'Ayló'chaxnim entered a 3:2 mean motion resonance with Venus located at 0.552 au that lasts for a 0.01 Myr before jumping in out of the resonance for the next ~ 0.1 Myr. (B) The evolution of the aphelion (orange) and perihelion (blue) distances of the same clone of 'Ayló'chaxnim representing the nominal orbit integrated to ± 10 Myr. The current aphelion (dashed line) and perihelion distances (dash-dotted line) are plotted as horizontal lines for Mercury (red), Venus (cyan), and Earth (purple). (C) Similar to B, but for a selected long-lived clone integrating its orbital evolution to 28 Myr. The aphelion and perihelion range of Mars is shown in black.

Venus, Earth, and Mars is similar to the published simulations of the general inner-Venus object population (Greenstreet et al. 2012).

3.3 Spectral type, dynamical pathway, and size

Spectroscopic observations of 'Ayló'chaxnim were made using the Keck telescope on 2020 January 23 indicating a reddish surface with colours in equivalent g (wavelength ~ 470 nm), r (wavelength ~ 620 nm), and i (wavelength ~ 750 nm) bandpasses of $g-r = 0.65 \pm 0.02$ mag, $r-i = 0.23 \pm 0.01$ mag. In addition, the surface of 'Ayló'chaxnim has a $i-z$ colour of 0.11 ± 0.02 mag where the equivalent z bandpass corresponds to a central wavelength of ~ 900 nm (Fig. 5). We interpret these as indicating a silicate S-type asteroid-like composition (Bus & Binzel 2002), consistent with an origin from the inner Main Belt, where S-type asteroids are most

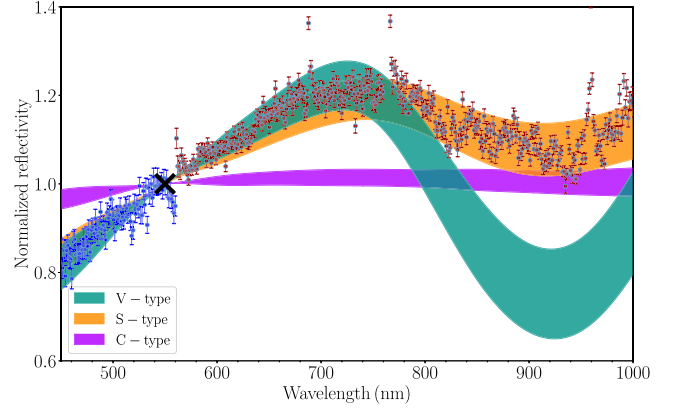


Figure 5. Visible wavelength reflectance spectrum of 'Ayló'chaxnim. Taken with the LRIS instrument on Keck I on 2020 January 23, the spectrum of 'Ayló'chaxnim is plotted as blue dots with 1σ uncertainty error bars. The spectrum has been normalized to unity at 550 nm indicated by the black cross. The spectrum was obtained by combining two spectra from the blue camera (blue data points) and the red camera (red data points). The data have been rebinned by a factor of 10 using an error-weighted mean. The dip at ~ 560 nm, spikes at ~ 770 nm, and ~ 960 nm are artefacts caused by the dichroic and imperfect removal of telluric H_2O absorption features. The spectral range of S, V, and C-type asteroids is overplotted.

abundant (DeMeo & Carry 2013). NEA models predict that asteroids with similar orbital elements to 'Ayló'chaxnim (table A1 and fig. A1, Bolin et al. 2022) originate from the inner Main Belt (Granvik et al. 2018).

One of the possible dynamical pathway for IVAs is to originate from the Main Belt through source regions located near various major planetary resonances (Granvik et al. 2017). If we assume that 'Ayló'chaxnim originated from the Main Belt as an asteroid family fragment (Bolin et al. 2017) before crossing inside of the orbit of Venus, asteroids with orbits similar to 'Ayló'chaxnim most likely originate from the ν_6 resonance, with a ~ 77 per cent probability, that forms the boundary of the inner Main Belt at 2.2 au (Morbidelli et al. 1994; Granvik et al. 2018). The second most likely source of 'Ayló'chaxnim with a ~ 18 per cent probability are the Hungaria asteroid population located just interior to the Main Belt at 2.0 au (Milani & Gronchi 2010) and the third most likely at ~ 4 per cent being the 3:1 mean motion resonance with Jupiter located in the Main Belt at 2.5 au (Wisdom 1983).

The typical albedo value for S-type asteroids is ~ 0.2 (Thomas et al. 2011; DeMeo & Carry 2013). In addition, we compared the source region probability for 'Ayló'chaxnim with the medium-resolution version of the NEA albedo (Morbidelli et al. 2020). The NEA albedo model predicts that ~ 60 per cent of kilometre-size inner-Venus objects should have albedos exceeding 0.2 (see fig. A3, Bolin et al. 2022) consistent with the albedo based on 'Ayló'chaxnim's taxonomic type. For an albedo of 0.2 and the absolute magnitude of 'Ayló'chaxnim, $H = 16.2 \pm 0.8$ mag taken from the JPL Small Body Database,³ we estimate that 'Ayló'chaxnim's diameter is $\sim 1.7 \pm 0.6$ km.

The number of IVAs in the NEA model brighter than 'Ayló'chaxnim's nominal value of $H = 16.2$ is 0.25. Using the range of H described by its 1σ uncertainty of 0.8, the number of objects brighter than the 1σ lower value of $H = 15.4$ is 0.05, and the number

³https://ssd.jpl.nasa.gov/tools/sbdb_lookup.html#/?sstr=594913

of objects brighter than the 1σ upper value of $H = 17.0$ is 0.7. Thus, the number of objects brighter than $H < 16.2 \pm 0.8$ is $0.25 \pm_{0.20}^{0.45}$ with the main source of uncertainty in the number of objects being due to the uncertainty on the H magnitude of 'Ayló'chaxnim. Thus, using the 1σ upper uncertainty value on H , and without taking into account small number statistics or observational selection effects, there is a $\sim 1-2\sigma$ difference between the discovery of 'Ayló'chaxnim and the NEA model.

4 DISCUSSION AND CONCLUSION

'Ayló'chaxnim seems like an ordinary NEA with a red colour and orbital evolution affected by planetary encounters. However, while asteroid population models predict that there are ~ 1000 km-scale NEAs, IVAs are scarce, representing less than 0.3 per cent of the NEA population (Granvik et al. 2018; Morbidelli et al. 2020). The detection of 'Ayló'chaxnim is surprising given its large size and the relative rarity of IVAs according to the NEA model. However, the twilight sky within 50 deg of the Sun is relatively unexplored and the comparison between observations and asteroid population models requires future exploration of this phase space. Observations of the near-Sun sky by current surveys such as ZTF and the Dark Energy Camera (Sheppard et al. 2021) along with future surveys such as the Rubin Observatory Legacy Survey of Space and Time (Bianco et al. 2022) will provide coverage of the near-Sun sky and the IVA population.

After this manuscript was accepted for publication, a manuscript was published by Ip et al. (2022) that also describes the discovery of 'Ayló'chaxnim.

ACKNOWLEDGEMENTS

The authors appreciate the help of Frank Masci with ZTF asteroid identification, Alessandro Morbidelli with synthetic populations, Palomar Observatory staff for help with ZTF operations, Jacqueline Serón, Carlos Corco, and Alfredo Zenteno with SOAR observations, Peter Senchyna, Alan Dressler, Carla Fuentes, Carlos Contreras, and Andy Monson with Magellan observations, R. Quimby, M. W. Coughlin and K. B. Burdge, M. J. Graham with follow up. CF acknowledges support from the Heising-Simons Foundation (grant #2018-0907). Part of this work was carried out at the Jet Propulsion Laboratory, California Institute of Technology, under contract with NASA 80NM0018D0004. This research has made use of data and/or services provided by the International Astronomical Union's Minor Planet Center and the Small-Body Database Lookup by the Jet Propulsion Laboratory Solar System Dynamics group. Based on observations obtained with the Samuel Oschin 48-inch Telescope at the Palomar Observatory as part of the Zwicky Transient Facility project. ZTF is supported by the National Science Foundation under Grant No. AST-1440341 and a collaboration including Caltech, IPAC, the Weizmann Institute for Science, the Oskar Klein Center at Stockholm University, the University of Maryland, the University of Washington, Deutsches Elektronen-Synchrotron and Humboldt University, Los Alamos National Laboratories, the TANGO Consortium of Taiwan, the University of Wisconsin at Milwaukee, and Lawrence Berkeley National Laboratories. Operations are conducted by COO, IPAC, and UW.

DATA AVAILABILITY

The data underlying this article will be shared on reasonable request to the corresponding author. The Twilight Survey data from 2019

September and 2020 January are available in ZTF Public Data Release 7.

REFERENCES

- Bellm E. C. et al., 2019a, *PASP*, 131, 018002
 Bellm E. C. et al., 2019b, *PASP*, 131, 068003
 Bianco F. B. et al., 2022, *ApJS*, 258, 1
 Binzel R. P., Reddy V., Dunn T. L., 2015, in Michel P., DeMeo F. E., Bottke W. F., eds, *Asteroids IV*. University of Arizona Press, Tucson, p. 243
 Bolin B. T., Delbo M., Morbidelli A., Walsh K. J., 2017, *Icarus*, 282, 290
 Bolin B. T. et al., 2020, *Minor Planet Electronic Circulars*, 2020-A99
 Bolin B. T. et al., 2022, *MNRAS*
 Bottke W. F., Jr, Vokrouhlický D., Rubincam D. P., Nesvorný D., 2006, *Annu. Rev. Earth Planet. Sci.*, 34, 157
 Bottke W. F., Morbidelli A., Jedicke R., Petit J.-M., Levison H. F., Michel P., Metcalfe T. S., 2002a, *Icarus*, 156, 399
 Bus S. J., Binzel R. P., 2002, *Icarus*, 158, 146
 Clemens J. C., Crain J. A., Anderson R., 2004, in Moorwood A. F. M., Iye M., eds, *Proc. SPIE Conf. Ser. Vol. 5492, Ground-Based Instrumentation for Astronomy*. SPIE, Bellingham, p. 331
 Coughlin M. W. et al., 2019, *MNRAS*, 485, 1412
 de la Fuente Marcos C., de la Fuente Marcos R., 2020, *MNRAS*, 494, L6
 Dekany R. et al., 2020, *PASP*, 132, 038001
 DeMeo F. E., Carry B., 2013, *Icarus*, 226, 723
 Duev D. A. et al., 2019, *MNRAS*, 486, 4158
 Duncan M., Levison H., Dones L., 2004, in Festou M. C., Keller H. U., Weaver H. A., eds, *Comets II*. University of Arizona Press, Tucson, p. 193
 Gaia Collaboration, 2016, *A&A*, 595, A1
 Gaia Collaboration, 2018, *A&A*, 616, A1
 Graham M. J. et al., 2019, *PASP*, 131, 078001
 Granvik M., Morbidelli A., Vokrouhlický D., Bottke W. F., Nesvorný D., Jedicke R., 2017, *A&A*, 598, A52
 Granvik M. et al., 2018, *Icarus*, 312, 181
 Greenstreet S., 2020, *MNRAS*, 493, L129
 Greenstreet S., Ngo H., Gladman B., 2012, *Icarus*, 217, 355
 Ip W. H. et al., 2022, *ApJ*, 935, L6
 Jedicke R., Bolin B., Granvik M., Beshore E., 2016, *Icarus*, 266, 173
 McCarthy J. K. et al., 1998, in D'Odorico S., ed., *Society of Photo-Optical Instrumentation Engineers (SPIE) Conference Series*, SPIE Conference Proceedings, p. 81
 Masci F. J. et al., 2019, *PASP*, 131, 018003
 Masi G., 2003, *Icarus*, 163, 389
 Milani A., Gronchi G. F., 2010, *Theory of Orbital Determination*. Cambridge Univ. Press, Cambridge
 Morbidelli A., Gonczi R., Froeschle C., Farinella P., 1994, *A&A*, 282, 955
 Morbidelli A., Delbo M., Granvik M., Bottke W. F., Jedicke R., Bolin B., Michel P., Vokrouhlický D., 2020, *Icarus*, 340, 113631
 Nesvorný D., Roig F., Ferraz-Mello S., 2000, *AJ*, 119, 953
 Oke J. B. et al., 1995, *PASP*, 107, 375
 Oszkiewicz D. A., Bowell E., Wasserman L. H., Muinonen K., Penttilä A., Pieniluoma T., Trilling D. E., Thomas C. A., 2012, *Icarus*, 219, 283
 Payne M., Rudenko M., Veres P., Bell D., Prema P., 2021, *Minor Planet Circulars*, p. 133823
 Perley D. A., 2019, *PASP*, 131, 084503
 Persson S. E. et al., 2013, *PASP*, 125, 654
 Popescu M. et al., 2020, *MNRAS*, 496, 3572
 Pravec P., Harris A. W., Kušnirák P., Galád A., Hornoch K., 2012, *Icarus*, 221, 365
 Rein H., Liu S.-F., 2012, *A&A*, 537, A128
 Rein H., Spiegel D. S., 2015, *MNRAS*, 446, 1424
 Sheppard S., Tholen D., Pokorny P., Kuchner M., Trujillo C., 2021, in *AAS Division of Planetary Science meeting #53, Bulletin of the American Astronomical Society*, Vol. 53, p. 306.22
 Thomas C. A. et al., 2011, *AJ*, 142, 85

- Tichá J., Noll K., Williams G., Chernetenko Y., Fernández J., Green D., Kilmartin Pam Nakano S., 2021, in Working Group on Small Body Nomenclature Bulletin, vol. 1, #11. IAU Working Group on Small Body Nomenclature, p. 14
- Tonry J. L. et al., 2012, *ApJ*, 750, 99
- Vereš P. et al., 2015, *Icarus*, 261, 34
- Warner B. D., Harris A. W., Pravec P., 2009, *Icarus*, 202, 134
- Whiteley R. J., Tholen D. J., 1998, *Icarus*, 136, 154
- Wisdom J., 1983, *Icarus*, 56, 51
- Ye Q. et al., 2020, *AJ*, 159, 70
- Zavodny M., Jedicke R., Beshore E. C., Bernardi F., Larson S., 2008, *Icarus*, 198, 284

SUPPORTING INFORMATION

Supplementary data are available at [MNRASL](#) online.

BTBAV2MNRAS_accepted_supplemental.pdf

Please note: Oxford University Press is not responsible for the content or functionality of any supporting materials supplied by the authors. Any queries (other than missing material) should be directed to the corresponding author for the article.

This paper has been typeset from a $\mathrm{T}_{\mathrm{E}}\mathrm{X}/\mathrm{L}^{\mathrm{A}}\mathrm{T}_{\mathrm{E}}\mathrm{X}$ file prepared by the author.